Journal of Materials Chemistry

Cite this: J. Mater. Chem., 2012, 22, 3059

www.rsc.org/materials

PAPER

Synthesis and structural, spectroscopic and nonlinear optical measurements of graphene oxide and its composites with metal and metal free porphyrins†

M. Bala Murali Krishna,[a] N. Venkatramaiah,[b] R. Venkatesan[b] and D. Narayana Rao*[a]

Received 27th September 2011, Accepted 2nd November 2011
DOI: 10.1039/c1jm14822b

In this paper we present the structure and spectroscopic, photophysical and nonlinear optical studies of covalently functionalized novel graphene oxide–[Cu, Zn, Sn, H_2 (metal free), VO] porphyrin composites. The composites were characterized by Field Enhanced Scanning Electron Microscopy (FE-SEM), micro-Raman, optical absorption, Fourier transform infrared (FT-IR), steady state and time resolved fluorescence spectroscopic techniques. The composites exhibit strong fluorescence quenching, suggesting strong electronic interactions between the porphyrin and graphene oxide molecules. Nonlinear optical absorption (NLA) studies of graphene oxide–porphyrin composites were investigated using the Z-scan technique at 532 and 800 nm with nanosecond (ns) and femtosecond (fs) laser pulses. Composites show strong two-photon absorption (TPA) as well as excited state absorption (ESA) leading to reverse saturable absorption (RSA) behaviour in the ns regime and saturable absorption (SA) behaviour was observed in fs regime. The metal free porphyrin–graphene oxide (GO) composite shows significant nonlinear absorption behaviour as well as highest fluorescence quenching behaviour compared to other GO–porphyrin composites. We further observed the enhanced figure of merit (FOM) values for composites in comparison with individual molecules.

Introduction

Graphene, a single 2D carbon sheet having sp^2 carbon atoms forming a honeycomb lattice, initiated enormous scientific interest since its discovery.[1] Its extraordinary electric, thermal and mechanical properties takes it ahead of other materials in terms of applications.[2–4] It was also predicted to be a plausible material for the construction of next-generation flexible solar-energy-conversion and optoelectronic devices that are low-cost, highly-efficient, thermally stable, environmentally friendly and lightweight.[5] Graphene has shown many unique properties like the quantum hall effect, good optical transparency, high Young's modulus, high carrier mobility and excellent thermal conductivity. Various forms of graphite, nanotubes and fullerenes can be viewed as derivatives of graphene. Despite many potential applications that graphene promises to offer, the processability of graphene is of critical importance in facilitating its integration with substrates and materials to ensure the stability and to preserve the integrity of the graphene materials. Hence, the attention is focused on the functionalization of graphene to improve its solubility/processability in both water and organic solvents.[6] Anchoring of different types of nanoparticles like Pd, Ag, Pt on reduced graphene oxide with controllable size leads to excellent performance in various oxidation reactions.[7,8] The covalent and non-covalent functionalization of graphene with different types of oligothiophenes exhibit high mobility and a superior optical limiting effect, better than that of the benchmark optical limiting material C_{60}.[9] Different types of covalently linked porphyrin/phthalocyanines–graphene hybrids exhibit remarkable competitive entry into the realm of light harvesting and solar energy conversion materials. Recent studies of functionalized graphene show that hybrid materials exhibit good NLA behaviour with high nonlinear optical absorption coefficients in ns and fs timescale regimes.[11–15] These properties make graphene an ideal photonic and optoelectronic material. It has been shown that porphyrins have many potential applications in optoelectronics, nonlinear optics,[16] as harvesters in solar cells, and in photodynamic therapy and optical limiting. Porphyrins

[a]School of Physics, University of Hyderabad, Hyderabad, Andhra Pradesh, 500046, India. E-mail: dnr.laserlab@gmail.com; dnrsp@uohyd.ernet.in
[b]Department of Chemistry, Pondicherry University, Puducherry, 605014, India

† Electronic supplementary information (ESI) available: FE-SEM micrographs of GO–Sn porphyrin, GO–Cu porphyrin composites, and graphite and graphene oxide are shown in Fig. S10–S11. Steady state emission and fluorescence quenching spectra of Zn porphyrin–GO, Sn porphyrin–GO, Cu porphyrin–GO, and VO porphyrin–GO are shown in Figs S1–S8. Time resolved fluorescence lifetime spectra of MH_2TP porphyrin, Sn porphyrin and Zn porphyrin are shown in Fig. S9. UV-Visible absorption spectra of pure porphyrins are shown in Fig. S12. Intensity dependent nonlinear Z-scan absorption curves for GO–H_2MHTP, GO–Cu porphyrin, GO–VO porphyrin, GO–Sn porphyrin and GO–Zn porphyrin are shown in Figs. S13 to S17. Energy level diagrams for GO, porphyrins and composites are shown in Fig. S19. Optical absorption and emission maxima, lifetimes of singlet states, quenching rate constants of pure porphyrin molecules are summarized in Table SA. See DOI: 10.1039/c1jm14822b

and graphene, having significant π-electron conjugation, are ideal to fulfil the requirement of a perfect nonlinear material. Through the conjugation of graphene with porphyrins, we have succeeded in enhancing the nonlinear optical coefficients of several graphene–porphyrin composites.[10] Since porphyrins/metalloporphyrins have strong electronic transitions in the visible and near infrared, their energies can be shifted by chemically modifying the ring or by changing the coordinated metal or both. Metal substituted porphyrins have shown better third order nonlinear optical properties than metal free porphyrins.[17–23] Therefore, it is timely and important to prepare various types of novel metalloporphyrins and modified porphyrins covalently linked to graphene for better optoelectronic and NLO materials. In this context, we explored the synthesis of novel covalent graphene oxide with different metalloporphyrins. In this paper we explored the nonlinear optical properties of graphene oxide with various metal porphyrins and metal free porphyrins in the fs regime and compared it with the long duration ns pulse excitations. We have observed that metal free porphyrins with graphene oxide show enhanced nonlinear absorption properties compared to graphene oxide with metal porphyrins in ns time scales. Unlike in nanosecond timescale results, we have observed saturable absorption (SA) behaviour in the fs open aperture Z-scan experiment. Absorption spectra revealed that this could be due to a low density of states at this wavelength. Therefore these graphene oxide composites can find applications as saturable absorbers in pulse shaping application.

Experimental details and results

1. Synthesis

1.1 Synthesis of 5-(*p*-hydroxyphenyl)-10,15,20-tritolylporphyrin [H_2MHTP]. This compound was synthesized from the corresponding 5-(*p*-methoxyphenyl)-10,15,20-tritolylporphyrin [H_2MMTP] by Adler's method.[24] 4-methoxy benzaldehyde (4 g, 33 mmol), 4-methylbenzaldehyde (7.7 mL, 66 mmol) and pyrrole (6.8 mL, 99 mmol) was added to 250 mL of propionic acid and brought to reflux for 2 h and allowed to cool overnight. The dark purple product was filtered and washed thoroughly with methanol until the filtrate became clear and the crude product was purified through column chromatography. The compound H_2MHTP was obtained by hydrolysis of the methoxy group using the known procedure as described earlier.[25]

1.2 Synthesis of Zn(II)MHTP and Cu(II)MHTP. This complex was obtained by refluxing H_2MHTP (0.5 mg, 0.07 mmol) in 50 mL of dimethylformamide with a saturated solution of M(II) acetate (M = Zn, Cu) in methanol for 1 h. The completion of the reaction was checked by thin layer chromatography and optical absorption spectrum. The reaction mixture was concentrated and purified through a silica gel column using chloroform as the eluant. Yield: 0.45 g (90%); IR (KBr): 3019, 2915, 1023 cm^{-1}.

1.3 Synthesis of Sn(IV)MHTP(OH)$_2$. $SnCl_2 \cdot 2H_2O$ (0.20 mg, 0.07 mmol) and H_2TPP (0.5 mg, 0.07 mmol) and sodium acetate (100 mmol) were refluxed in 100 mL of glacial acetic acid for 6 h. An additional amount of 10 mmol of $SnCl_2 \cdot 2H_2O$ was added to the reaction mixture and refluxed for an additional 6 h. The reaction mixture was cooled to room temperature and the reaction mixture was concentrated to dryness under vacuum at 30 °C. The residue was dissolved in a small volume of chloroform and purified over a silica gel column using 2% chloroform in benzene. The eluant was filtered and dried. The residue was dissolved in a 1 : 1 mixture of chloroform and acetone. This mixture was treated with a few mL of concentrated HCl and it was stirred for 1 h. The final solution was washed with water and dried under vacuum and the complex further recrystallised from a 1 : 1 mixture of chloroform and petroleum ether. Yield: 60%. A similar methodology was adopted for the synthesis of VO(II) MHTP by taking $VO(acac)_2$ and H_2MHTP as the starting materials.

1.4 Synthesis of graphene oxide (GO) from graphite. Graphene oxide was prepared using a modification of Hummers and Offeman's method.[26–28] Briefly in a typical reaction, 1 g graphite, 1 g $NaNO_3$, and 50 mL H_2SO_4 were stirred together in an ice bath. $KMnO_4$ (3 g) was slowly added while stirring, and the rate of addition was controlled to prevent the mixture temperature from exceeding 20 °C. The mixture was then transferred to a 35 °C water bath and stirred for about 1 h, forming a thick paste. Subsequently, 50 mL de-ionized water was added gradually and the temperature was raised to 98 °C. The mixture was further treated with 150 mL de-ionized water and 10 mL 30% H_2O_2 solution. The warm solution was then filtered and washed with de-ionized water until the pH was 7 and dried at 65 °C under vacuum.

1.5 Synthesis of GO–COOH. 0.5 g of graphene oxide (GO) was loaded in a 100 mL round-bottomed flask and 50 mL de-ionized water was added and stirred for 1 h and sonicated for 30 min. To the resulting solution, 5 mL of 50% hydrazine hydrate was gradually added and refluxed at 100 °C for 4 h. The resulted solution was filtered and washed thoroughly with anhydrous tetrahydrofuran (THF) and dried under vacuum for 24 h.

1.6 Synthesis of GO–COCl. GO–COOH (0.5 g) was suspended in $SOCl_2$ (30 mL) and 5 mL of DMF was added and refluxed at 70 °C for 24 h under nitrogen atmosphere. The resultant solution was filtered and washed with anhydrous tetrahydrofuran (THF) and dried under vacuum, yielding acylated graphene oxide (GO–COCl) (0.4953 g).

1.7 Synthesis of covalently attached porphyrin graphene oxide hybrids. A mixture of GO–COCl (30 mg) and H_2MHTP (60 mg) were taken in a 100 mL round bottom flask and 3 mL of triethylamine and 15 mL of DMF were added and heated to 80 °C for 72 h under a nitrogen atmosphere, and an additional 6 h with intermittent sonication to give a homogeneous black dispersion. After the reaction, the solution was cooled to room temperature, and then poured into diethyl ether (300 mL) to precipitate the product. The precipitate was collected by centrifuging at 8000 rpm for 0.5 h. The supernatant which contained dissolved H_2MHTP was discarded and the precipitate was washed thoroughly. After adding another 100 mL of diethyl ether, the mixture was sonicated for 5 min and then centrifuged at 8000 rpm for 0.5 h to collect the H_2MHTP–GO, discarding the supernatant. Finally, the precipitate was washed with $CHCl_3$ five

times following the above procedure. UV–Vis spectra and thin layer chromatography (TLC) were used to check the supernatant layer to ensure no H_2MHTP existed in the final washing. This methodology was implemented for metalloporphyrin–graphene oxide composites [metal = Zn, Cu, Sn(IV)]. We defined Zn porphyrin, Cu porphyrin VO porphyrin and Sn porphyrin as Zn (II)MHTP, Cu(II)MHTP, VOMHTP, and Sn(IV)MHTP$(OH)_2$, respectively throughout the article. The synthesis scheme of covalently linked GO–porphyrin composites is shown in Fig. 1.

2. Structural and spectroscopic characterization

2.1 Field enhanced-scanning electron microscopy (FE-SEM) studies. The scanning electron micrographs for the GO–porphyrin hybrid materials demonstrate that a homogeneous system with a micrometre order of magnitude was obtained. FE-SEM images of graphene oxide–porphyrin composites were recorded using a Carl-Zeiss Ultra 55 model. Fig. 2 shows the selected micrographs for GO–H_2MHTP and the GO–Zn porphyrin. The GO–Cu porphyrin, GO—Sn porphyrin, graphite and graphene oxide micro graphs are shown in the ESI.† Pure graphite exhibits ordered flakes of a 4–5 μm range. On functionalization, GO exhibits a three-dimensional network of randomly oriented sheet-like structures with a wrinkled texture and hierarchical pores with a wide size distribution. It is clearly seen from the top-view image that the composites have a uniform and dense surface, composed of plate-like particles with slightly scrolled edges ranging from several tens of nanometres to several hundreds of nanometres in the lateral dimension. Some GO flakes of composites fold together and represent crinkly sheets. The surface is much rougher than that of GO which can be attributed to the covalent linkage of porphyrins to the GO sheet.

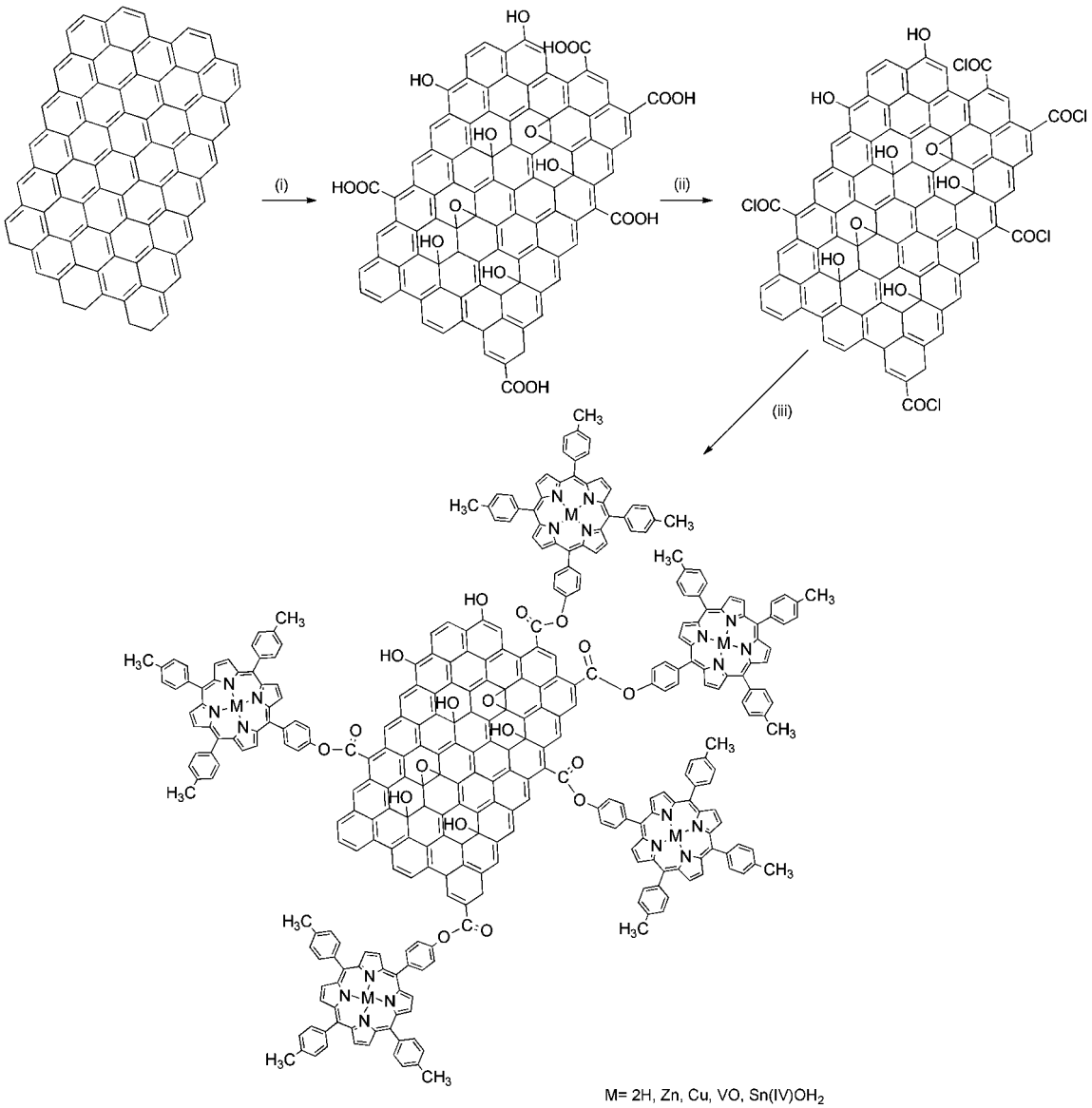

Fig. 1 Synthesis scheme of novel graphene oxide–(H_2, Cu, Zn, VO, Sn$(OH)_2$) porphyrin composites (i) $NaNO_3$, H_2SO_4/$KMnO_4$, 1 h, $N_2H_4 \cdot 2H_2O$,100 °C, 4 h (ii) $SOCl_2$/DMF, 70 °C(III) Et_3N/DMF, 80 °C, 72 h.

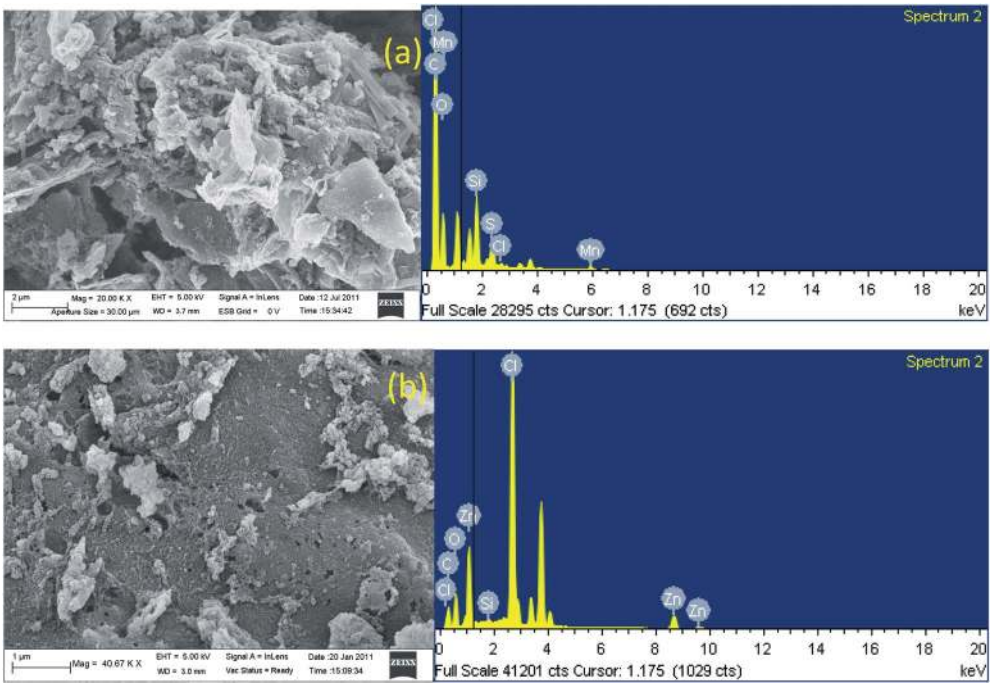

Fig. 2 FE-SEM and EDS images of a) GO–H_2MHTP and b) GO–Zn porphyrin composite.

2.2 Micro-Raman studies. Raman spectroscopy is a versatile and non-destructive characterization technique for obtaining information on the nature of binding of these polyaromatic hydrocarbons. Raman spectra were recorded at room temperature using a micro-Raman spectrometer (LABRAM-HR) with a laser excitation of 514.5 nm. As can be seen in Fig. 3, the Raman spectrum of pure graphite exhibits a characteristic peak at 1591 cm^{-1}, corresponding to the G band of ordered sp^2-bonded carbon atoms. As per the spectrum of GO, (Fig. 3) GO exhibits a D-band at 1345 cm^{-1} due to edges, other defects, and disordered carbon. The G-band appearing at 1575 cm^{-1} is broadened and blue shifted slightly while the intensity of the D band increases substantially. These phenomena could be attributed to the significant decrease in the size of the in-plane sp^2 domains due to oxidation. It is well known that the increased intensity ratio of D : G accounts for a lower degree of crystallinity of graphite materials.[29] The functionalized GO with various porphyrins results in small changes in the D and G peaks. When the Raman spectra of GO–porphyrins were compared with that of GO, subtle rather than drastic changes were observed. The G band shifted upward from 1575 to 1583 cm^{-1}, which might be caused by the increasing number of layers in their solid states. As porphyrins are covalently linked to GO, they can absorb on both sides of the graphene sheets. The weak π–π stacking interaction with porphyrins can occur between two monolayer sheets in the same way as the anchoring of phenyl rings on one GO sheet.[30] The intensity ratio of D : G bands increased from 0.932 for GO to 0.982 for GO–Cu porphyrin, 0.956 for GO–Zn porphyrin and 0.978 for GO–Sn porphyrin. However, the ratio of the D : G band intensity decreased for GO–H_2MHTP hybrids (0.89). This indicates that some of the oxygenated groups lead to the re-established conjugated graphene network.

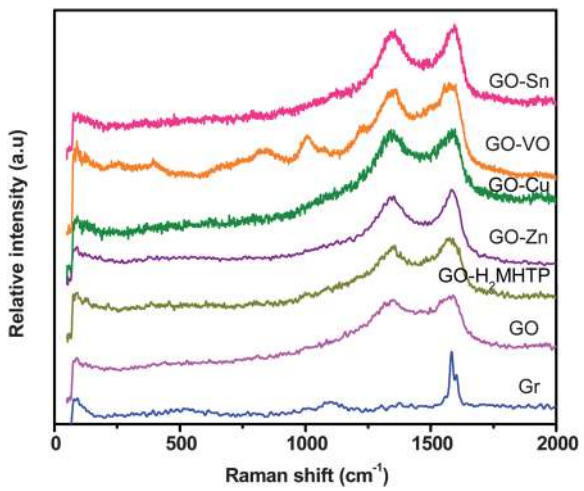

Fig. 3 Micro-Raman studies of graphite, graphene oxide, graphene oxide–H_2MHTP, graphene oxide–Zn porphyrin, graphene oxide–Cu porphyrin, graphene oxide–VO porphyrin and graphene oxide–Sn porphyrin composite.

2.3 Linear optical absorption studies. The optical absorption measurements were carried out by UV-Visible spectrometry (JASCO V-670). Fig. 4 shows optical absorption spectra of composite materials, H_2MHTP and graphene oxide molecules. Graphene oxide shows an absorption peak at 268 nm which agrees with the literature value.[31] The copper porphyrin peak at 421 nm is enhanced in the graphene oxide–copper porphyrin composite while the zinc porphyrin peak at 429 nm gets suppressed in the graphene oxide–zinc porphyrin composite material. The H_2MHTP absorption peak at 420 nm completely vanishes in the graphene oxide–H_2MHTP composite. Similarly,

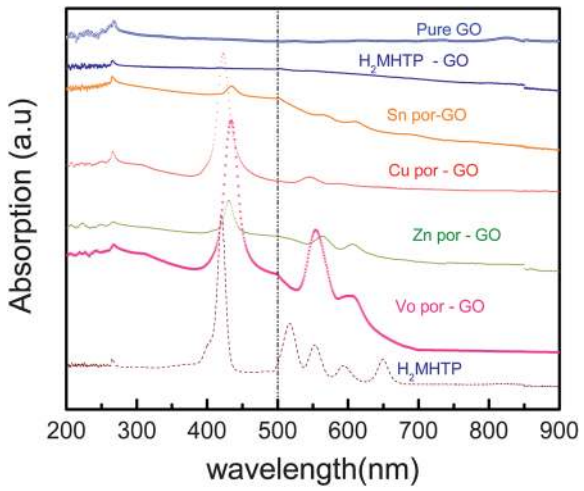

Fig. 4 UV-visible absorption spectra of pure graphene oxide, graphene oxide–copper porphyrin composite, graphene oxide–zinc porphyrin composite, graphene oxide–tin porphyrin composite, H_2MHTP, and graphene oxide–H_2MHTP composite in DMF. The absorbance in the region 500 nm to 890 nm is multiplied by 10 times to have more clarity near the excitation wavelengths.

the Sn porphyrin has an absorption peak at 432 nm which is suppressed in the graphene oxide–Sn porphyrin composite. These observations indicate the formation of composites and also the tunability of optical properties through different substitutes in porphyrin molecules. Porphyrins exhibit several peaks near the wavelength of 532 nm, whereas they almost disappear in the composites. The absorbance in the region 500 nm to 900 nm (Fig. 4) is amplified by 10 times for clear visibility. 0.2 mg mL^{-1} of graphene oxide–porphyrin composites were taken for Z-scan experiments. We estimated the porphyrin and graphene oxide contents in the composite as 0.037 mg mL^{-1} (5×10^{-5} M) and 0.163 mg mL^{-1}, respectively.[10] Linear transmittances of graphene oxide, copper porphyrin, zinc porphyrin, Sn porphyrin, H_2MHTP, VO porphyrin and graphene oxide–copper porphyrin, graphene oxide–zinc porphyrin, graphene oxide–Sn porphyrin, graphene oxide–H_2MHTP, and graphene oxide–VO porphyrin composites were 85 (0.71), 97 (0.13), 87 (0.61), 84 (0.77), 82 (0.61), 79 (1.05) 75 (1.26), 80 (0.99), 68 (1.65), 60 (2.22) and 60.8% (2.16 cm^{-1}) respectively at 532 nm and 77 (1.12), 91 (0.40), 93 (0.32), 92 (0.37), 92 (0.37), 92 (0.37), 77 (1.16), 82 (0.88), 76 (1.19), 67 (1.76) and 74% (1.3 cm^{-1}) respectively at the 800 nm wavelength (with the corresponding optical densities given in brackets).

2.4 Fourier transform infrared spectroscopy (FT-IR). The FT-IR spectra were recorded using KBr plates in the range 500–4000 cm^{-1} using a Nicolet 6700 FT-IR spectrometer. Fig. 5 shows the typical FTIR spectrum obtained for our graphite oxide material. The most characteristic features are the broad, intense band at 3430 cm^{-1} (O–H stretching vibrations) and the bands at 1725 cm^{-1} (C═O stretching vibrations from carbonyl and carboxylic groups), 1639 cm^{-1} (skeletal vibrations from unoxidized graphitic domains), 1380 cm^{-1} (C–OH stretching vibrations), and 1027 cm^{-1} (C–O stretching vibrations). The appearance of the peaks at around 2900 cm^{-1} is ascribed to the aromatic stretching vibrations of C–H bonds of GO. After covalent functionalization with porphyrins, a new peak appears at ~1582 cm^{-1} corresponding to the C═C vibrations of porphyrins and the peak of the C–O stretching vibration shifts to 1108 cm^{-1}, and broadens. The peak present at ~1707 cm^{-1} is assigned to the bending vibration of the C═N of the porphyrin ring. The disappearance of the peak at 1380 cm^{-1} clearly indicates that in porphyrin–GO composites, the porphyrin molecules are covalently bonded to the graphene oxide *via* carboxylic acid linkage. However, the appearance of sharp intense peaks at 1390 cm^{-1} and 793 cm^{-1} for Sn porphyrin–GO composites are due to the axial Sn–OH stretching and bending vibrations. VO porphyrin–GO composites show more broadened –OH stretching vibrations than the other composites.

2.5 Steady state fluorescence studies. The electronic interaction between the various porphyrins units covalently with GO is studied through steady state and time resolved fluorescence techniques. Steady state fluorescence emission was performed with a Spex FluoroLog-3 spectrofluorometer (Jobin Yvon) equipped with a Hamamatsu R928 photomultiplier tube and a resolution of ±1 nm. On excitation at $\lambda_{ex} = 420$ nm (Fig. 6), GO–H_2MHTP exhibits emission peaks at 650 and 718 nm which arise due to a $S_1 \rightarrow S_0$ transition. The emission intensity of H_2MHTP is decreased by 21% as compared to the control sample (which is prepared with the pure porphyrin so that the control sample has the same absorbance value as that of the composite,

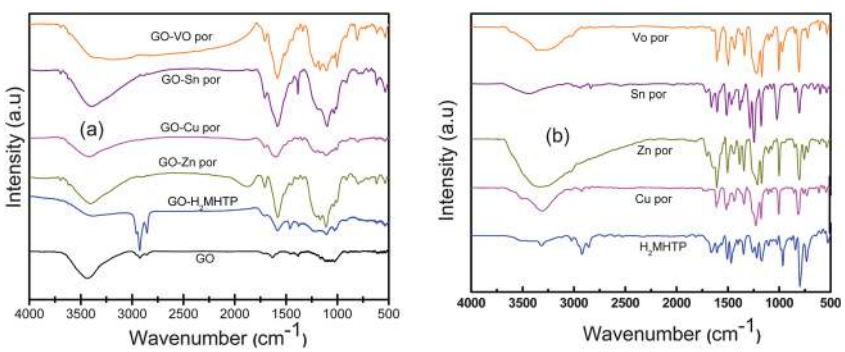

Fig. 5 FT-IR spectra of a) graphene oxide, graphene oxide–H_2MHTP, graphene oxide–Zn porphyrin, graphene oxide–Cu porphyrin, graphene oxide–Sn porphyrin, graphene oxide–VO porphyrin composite and b) H_2MHTP, Cu porphyrin, Zn porphyrin, Sn porphyrin, and VO porphyrin molecules.

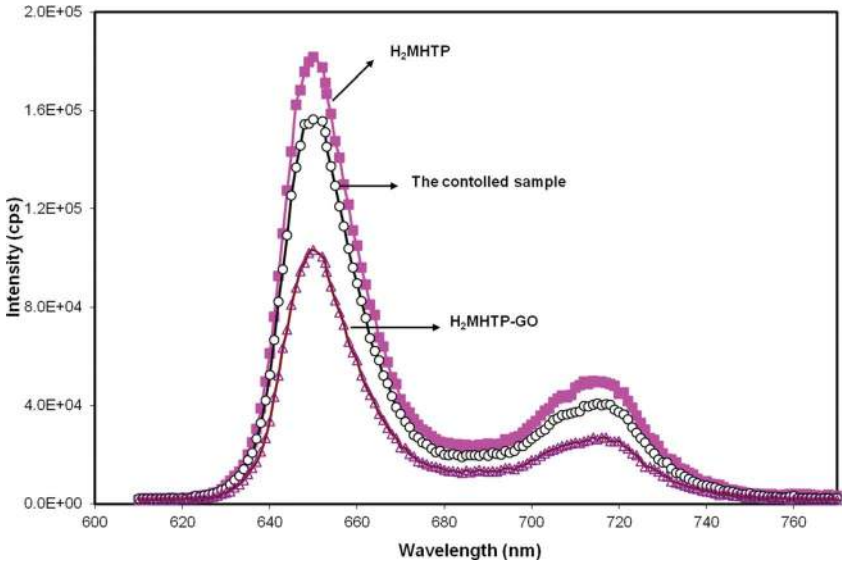

Fig. 6 Steady state emission spectra of H_2MHTP, the control sample, and H_2MHTP–GO in chloroform, with normalization of the absorbance of the Soret band excitation wavelength (420 nm) to the same value (0.18).

that is 0.18) indicating that H_2MHTP–GO undergoes fluorescence quenching. The effective emission quenching of porphyrin in GO–H_2MHTP composites is indicative of electronic interactions between the singlet excited state of the porphyrin ($^1H_2$MHTP*) and GO. Therefore, covalently linked H_2MHTP with GO can act as an energy absorbing and electron transporting antenna, while GO acts as an electron acceptor unit, in this hybrid system where the porphyrin moiety resides near the surface of the GO framework. It is also interesting to note that with an increase in the concentration of GO–H_2MHTP (wt mL^{-1}), the fluorescence emission intensity decreases gradually without any change in the spectral pattern indicating that the composites undergo self-quenching as shown in Fig. 7. About 27% quenching is observed for H_2MHTP–GO (0.2 mg mL^{-1}) with a highest quenching constant of 3.57×10^9 S^{-1}. However, Zn porphyrin–GO exhibits better quenching at 21% (for 2 mg mL^{-1}) among other metalloporphyrin–GO composites with a quenching constant of 3.16×10^9 S^{-1}. Similar results were observed in other porphyrin–GO composites and the pertinent data is summarized in Table 1. All the metalloporphyrins (M = Zn, Sn(IV),VO and Cu) exhibit $S_1 \rightarrow S_0$ emission at ~595 and ~653 nm as shown in Fig. 8. The intensity of the $S_1 \rightarrow S_0$ emission is found to vary with the metal centre. GO–Cu porphyrin and GO–VO porphyrin exhibit weak emission. In contrast to GO–H_2MHTP, GO–Zn porphyrin and GO–Sn porphyrin exhibit $S_2 \rightarrow S_0$ emission peaks at 472 nm and 483 nm. In porphyrin–GO hybrids, after photo excitation, donor–acceptor interaction between the two moieties of H_2MHTP (Zn porphyrin) and GO includes an inter-molecular charge transfer from the photo excited singlet H_2MHTP to the graphene oxide moiety, and this results in the observed fluorescence quenching and energy release. Hence, they can be used as sources for solar energy harvesting in solar cells.

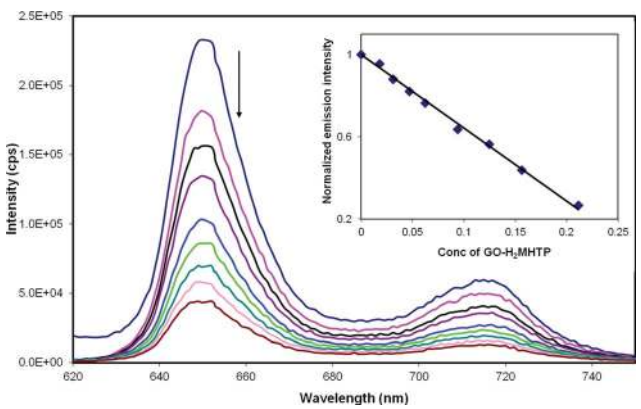

Fig. 7 Fluorescence quenching behaviour of GO–H_2MHTP. Inset shows emission normalized intensity with respect to concentration of the graphene oxide–H_2MHTP composite.

2.6 Time-correlated single photon counting (TCSPC) studies. To understand further the energy transfer between GO–porphyrins, the fluorescence lifetime studies were carried out with TCSPC using 460 nm LED with a FWHM of 1.3 ns. The fluorescence lifetime decay profiles are presented in Fig. 9. The fluorescence lifetime of GO–H_2MHTP shows single exponential decay with a lifetime of 6.4 ns. However, H_2MHTP exhibits a lifetime of 9.1 ns in chloroform solution. The significant decrease in the lifetime indicates that charge-separation and/or electron transfer scenario in the GO–H_2MHTP *via* ($^1H_2$MHTP*). This further supports the fluorescence quenching behaviour of GO–H_2MHTP shown in Fig. 7. The $S_1 \rightarrow S_0$ fluorescence lifetime of metalloporphyrins were also estimated and the data is presented in the Table. 1.

3. NLO measurements

The ns laser source was a frequency doubled Nd:YAG laser (INDI-40, Spectra-Physics) with a 6 ns pulse duration and a repetition rate of 10 Hz at a 532 nm wavelength. The fs laser was a Spectra-Physics Ti-sapphire regenerative amplifier with

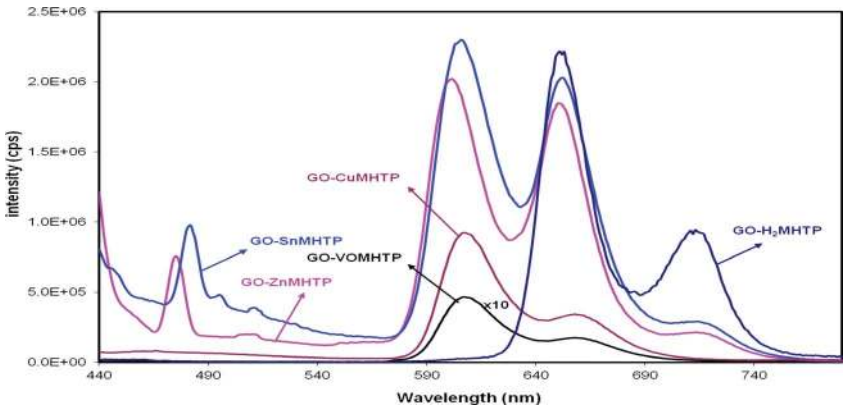

Fig. 8 Fluorescence studies of graphene oxide–H_2MHTP, graphene oxide–Zn porphyrin, graphene oxide–Sn porphyrin, graphene oxide–Cu porphyrin and graphene oxide–VO porphyrin composites (spectra for graphene oxide–VO porphyrin is amplified by 10 times).

a 100 fs pulse duration and operated at 1 KHz repetition rate and 800 nm wavelength. Graphene oxide, porphyrins and their composites are taken as solutions in DMF for the experimental studies. Open aperture Z-scan studies were carried out by focusing the input beam on to the sample using a lens of 120 mm focal length forming 27 μm and 40 μm spot sizes at the focus in ns and fs regimes respectively. The transmitted light was collected with a photodiode. The peak intensities, I_{00}, estimated at the focus in Z-scan experiments were 300 MW cm^{-2} in ns experiments and 300 GW cm^{-2} in fs experiments.

Fig. 10 (a) shows typical open aperture Z-scan curves for pure graphene oxide, H_2MHTP, Sn porphyrin, VO porphyrin, graphene oxide–H_2MHTP, graphene oxide–Sn porphyrin and graphene oxide–VO porphyrin composites. Curves for pure porphyrins, graphene oxide and composites show RSA behaviour in the ns regime and composites show strong SA behaviour in the fs time scales. To understand our observations, we followed the rate equation model. For graphene oxide–metal porphyrin composite materials we proposed a simplified model as in our earlier report.[10] The same model is used to fit the open aperture Z-scan curves with ns pulses. With fs pulses, for porphyrins the intersystem crossing rate from singlet to triplet state is a slower process compared to excitation pulse width and the generalized five level models for porphyrins effectively becomes three level. From the absorption spectra it is very clear that due to the absorption band at 268 nm, the incident 532 nm laser beam can undergo TPA. Also because of the weak linear absorption at the excitation wavelengths, the incident laser beam can undergo one-photon absorption. Because of the very broad absorption spectrum exhibited by the graphene oxide molecule, the levels at 268 nm show fast relaxations. Porphyrins are known to show strong ESA and TPA. A good energy transfer from the excited states of porphyrins to the GO band, leads to enhancement of the TPA of the porphyrins and at the same time the GO excited states relax fast to the ground state through the continuous band structure. Because of the good overlap and energy transfer between the porphyrin and the GO energy levels, we assume a model with three levels: the ground state, first excited state of the porphyrin together with the absorbing levels of GO at 532 nm, and higher excited states of the porphyrin and GO as the third (shown at extreme right of the Fig. S19, ESI),† for the graphene oxide–porphyrin composites to simplify the analysis of the otherwise complex data. GO is a non-stoichiometric compound, so it has no constant molecular weight. It is impossible to estimate the σ_0 from the formula $\sigma_0 = \alpha/N$ where $N = N_A \times C$. N_A is Avogadro's number and C is the concentration of the compound. As one can't determine the concentration, there is no easy way to estimate the σ_0 from any formulae. Therefore, we have tried to estimate σ_0 from theoretical modelling. The generalized rate equations for graphene oxide, porphyrins and composites are

$$\frac{\partial N_1}{\partial t} = -\frac{\sigma_0 I N_1}{\hbar\omega} - \frac{\beta I^2}{2\hbar\omega} + \frac{N_2}{\tau_{s_1}} \quad (1)$$

$$\frac{\partial N_2}{\partial t} = \frac{\sigma_0 I N_1}{\hbar\omega} - \frac{\sigma_1 I N_2}{\hbar\omega} - \frac{N_2}{\tau_{s_1}} + \frac{N_3}{\tau_{s_n}} \quad (2)$$

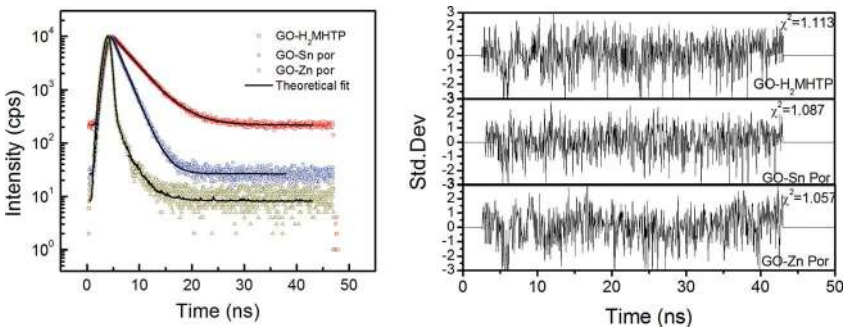

Fig. 9 The fluorescence lifetime decay of various GO-porphyrin composites.

Table 1 Optical absorption and emission maxima, lifetime of singlet state, quenching rate constant of graphene oxide–H_2MHTP, graphene oxide–Zn porphyrin, graphene oxide–Cu porphyrin, graphene oxide–Sn porphyrin and graphene oxide–VO porphyrin composite

	Absorption		Steady state emission			
Samples	Soret Band (nm)	Q-band (nm)	λ_{ex} (nm)	λ_{em} (nm)	Lifetime (ns)	k^s_q (s^{-1})
GO–H_2MHTP	425	516, 551, 592, 648	420	650, 718	6.4	3.57×10^9
GO–Zn porphyrin	431	564, 606	420	472, 592, 652	1.41	3.16×10^9
GO–Cu porphyrin	423	545	420	594, 649	——	1.08×10^9
GO–Sn porphyrin	435	568, 612	420	483, 599,654	4.06	2.57×10^9
GO–VO porphyrin	434	554, 606	420	593, 647	——	1.05×10^9

$$\frac{\partial N_3}{\partial t} = \frac{\sigma_1 I N_2}{\hbar\omega} + \frac{\beta I^2}{2\hbar\omega} - \frac{N_3}{\tau_{s_n}} \quad (3)$$

where N_j is the population per cubic centimetre of state S_j, while $j = 1,2,3$. $\hbar$ is the reduced Planck constant, ω is the laser frequency and τ_{s_i} is the lifetime for state S_i, while $i = 1, n$. Where $I = I_{00}\left(\frac{\omega_0^2}{\omega^2(z)}\right)\exp\left(-\frac{t^2}{\tau_p^2}\right)\exp\left(-\frac{2r^2}{\omega^2(z)}\right)$ and $\omega(z) = \omega_0(1 + (z/z_0)^2)^{1/2}$; z varies from −2 to +2 cm. I_{00} is the peak intensity at focus of Gaussian beam. $z_0 = \frac{\pi\omega_0^2}{\lambda}$, $\omega_0 = \frac{4\lambda f}{\pi d}$, τ_p is the input pulse width, z_0 is the Rayleigh range, λ is the wavelength, ω_0 is beam waist, f is the focal length of the lens and d is the diameter of the laser beam before the lens. For graphene oxide and porphyrins, intensity transmitted through the sample is given by Beer's law

$$\frac{\partial I}{\partial z} = -(\sigma_0 N_1 + \sigma_1 N_2 + \beta I)I \quad (4)$$

where σ_0, σ_1 and β are ground state absorption cross section, excited state absorption cross section and two-photon absorption coefficient respectively.

For the composite molecules, σ_1 is taken as the effective excited state absorption cross section which includes $S_1 \rightarrow S_n$ and $T_1 \rightarrow T_n$ of porphyrin molecules and $S_1 \rightarrow S_n$ of graphene oxide molecules and β is taken as the effective TPA coefficient for both graphene oxide and porphyrin molecules. Fig. 10 (a) also shows theoretical fits, which match quite well with the experimental data. From the fit, we derive σ_0, σ_1, and β. τ_{s_1} and τ_{s_n} for pure graphene and porphyrins are taken from the reported literature.[32–35] These parameters are compared for different molecules and the composites in Table 2. One can observe that β_{por} for porphyrin is much smaller than β_{gr} and β_{comp} in the ns regime. Fig. 10 (b) shows the intensity dependent nonlinear optical transmission of the graphene oxide–H_2MHTP composite at focus (corresponding intensity dependent open aperture Z-scan curve is shown in Fig. S13, ESI).† It confirms that the obtained nonlinear coefficient values remain constant in the intensity range from 12 MW cm^{-2} to 300 MW cm^{-2}. The optical limiting curves are plotted and shown in Fig. 11 for the Cu porphyrin, pure graphene oxide and graphene oxide–porphyrin composite materials in nanosecond time scales. Compared to individual porphyrin and graphene oxide, composite molecules show better limiting behaviour. We estimated the figure of merit for pure porphyrins, and composite materials and they are shown in Table 2. Capability of a material for optical limiting can be described by the FOM ($=\sigma_{ex}/\sigma_0$), where σ_{ex} and σ_0 are the excited state and ground state absorption cross sections. We estimated the limiting thresholds of VO porphyrin, Sn porphyrin, H_2MHTP, graphene oxide–VO porphyrin, graphene oxide–Sn porphyrin and graphene oxide–H_2MHTP as 0.8, 0.9, 1.1, 0.32, 0.45 and 0.25 J cm^{-2}, respectively. While the current studies

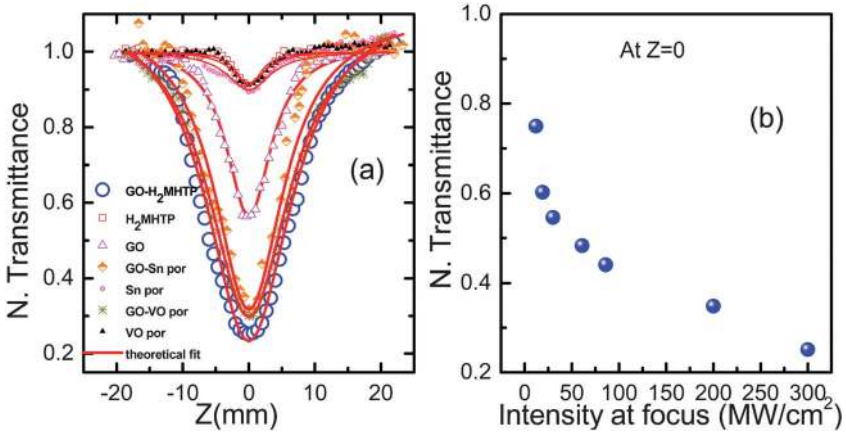

Fig. 10 (a) Open aperture Z-scan curves of H_2MHTP, graphene oxide–H_2MHTP composite, Sn porphyrin, graphene oxide–Sn porphyrin composite, VO porphyrin, graphene oxide–VO porphyrin composite and pure graphene oxide in DMF with a peak intensity of (I_{00}) 0.3 GW cm^{-2} at 532 nm in the ns regime. The red line represents the theoretical fit. (b) Intensity dependent normalized transmittance at focus for graphene oxide–H_2MHTP composite material.

Table 2 Excited state and ground state parameters β, σ_1, σ_1/σ_0, τ_1 and τ_2 of VO porphyrin, Sn porphyrin, H_2MHTP, graphene oxide–VO porphyrin, graphene oxide–Sn porphyrin and graphene oxide–H_2MHTP composite in the ns regime

Samples	β (cm GW^{-1})	σ_1 (cm^2) $\times 10^{-19}$	FOM (σ_1/σ_0)	τ_1 (ns)	τ_2 (ps)
VO porphyrin	142	84	17.5	1.3	2.2
Sn porphyrin	168	102	22.7	4.1	2.3
H_2MHTP	159	98	20.9	9.2	2.8
GO–VO porphyrin	3760	262	30.1	1.2	0.55
GO–Sn porphyrin	3650	248	29.2	4.06	0.6
GO–H_2MHTP	4920	412	46.8	6.4	0.65

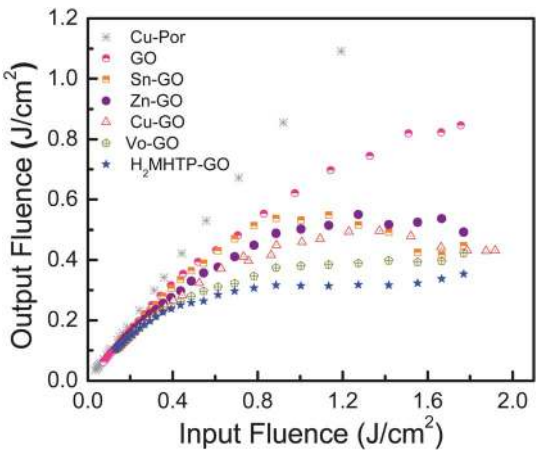

Fig. 11 Optical limiting behaviour of graphene oxide–porphyrin composites at 532 nm wavelength, in the ns regime.

involve a larger number of metal porphyrins, their composites with GO, and a comparison with metal free porphyrin with GO, the nanosecond limiting thresholds and excited state parameters of graphene oxide, graphene oxide–zinc porphyrin and graphene oxide–copper porphyrin composites are taken from the earlier reports.[10] Composites exhibit enhanced optical limiting behaviour which arises from ESA, TPA and nonlinear scattering. It is important to notice that behaviour of the curves is quite different at ns (532 nm) and fs (800 nm) time scales. In ns time scales, excitation at 532 nm has a very strong TPA in graphene oxide and it dominates both in pure graphene oxide and the composites. From our experimental observations, metal free porphyrins with graphene oxide show enhanced nonlinear absorption behaviour compared to metal porphyrins with graphene oxide. Previous NLA results on metal porphyrins show high nonlinearities due to metal substituents in the core of porphyrin molecules, whereas in our results graphene oxide plays superior role than metal substitutes. Graphene oxide completely dominates as a good electron acceptor. GO–H_2MHTP show higher β, ESA than GO–metal porphyrins. However at fs time scales, we have introduced saturation for ground state absorption to fit the SA behaviour open aperture Z-scan curves. Excitation at 800 nm has a very poor TPA cross section for graphene oxide. We recorded the pure solvent contribution and the nonlinear absorption when porphyrins, graphene oxide and the composites are dissolved in DMF solution in order to estimate the effect of the solvent, while

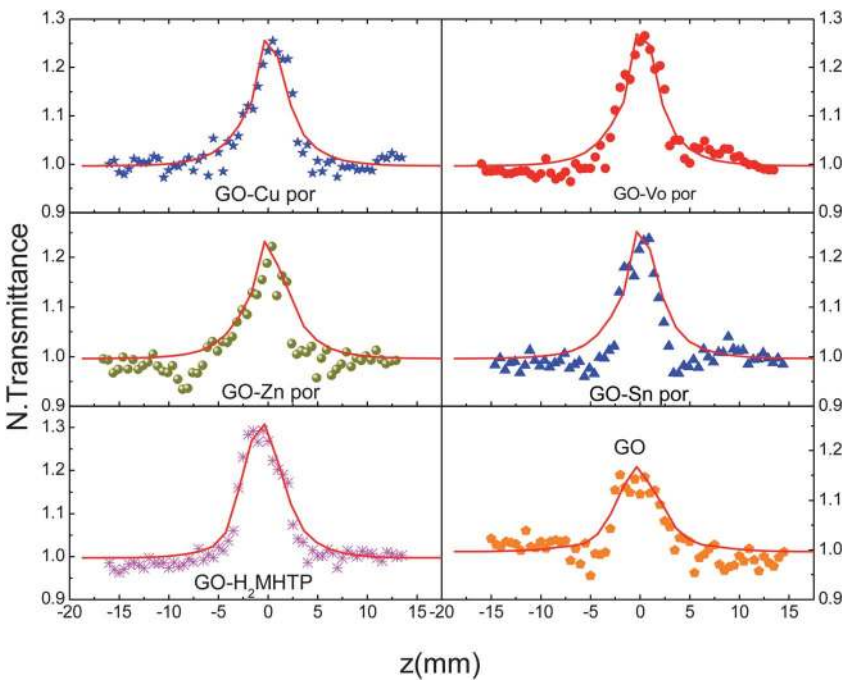

Fig. 12 Open aperture Z-scan curves for pure graphene oxide and graphene oxide–porphyrin composites at 800 nm wavelength, in the fs regime.

with graphene oxide and the composites the curves exhibit shallower depths in the RSA curves shown in Fig. S18 of the ESI.† This is explained as being due to the opposite nature of nonlinear absorption properties of graphene oxide and its composites in comparison to the DMF solvent. DMF has strong TPA/3PA at higher intensities while graphene oxide and the composites show SA behaviour at fs time scales with an excitation wavelength of 800 nm. When the transmission curves are divided by the pure solvent curve to eliminate the effect of solvent, we observe SA behaviour for both graphene oxide and composites as shown in Fig. 12. In our experiment we observe RSA curves for graphene oxide and graphene oxide composites at 800 nm while the earlier report[32] shows SA behaviour at 790 nm, 80 fs laser excitation. However both results are in good agreement when we eliminate the solvent contribution. The TPA coefficient (β) for graphene oxide composites is of the order 10^{-11} cm W^{-1} with the highest value of 1.37×10^{-11} cm W^{-1} for the graphene oxide–Cu porphyrin composite compared to other composites. FS results suggest that graphene oxide composites act as good saturable absorbers, which can replace traditional saturable absorbers for different applications like pulse shaping and shutters in fs systems.

Conclusions

We have studied structural, spectroscopic and nonlinear optical properties of porphyrins (Cu, Zn, Sn, H_2MHTP, VO) and their covalently linked composites with graphene oxide. Conjugation of porphyrins and graphene oxide was confirmed by optical absorption, FT-IR and FE-SEM studies. Fluorescence quenching in composites suggests the strong electronic interaction between porphyrin and graphene oxide excited states. This interaction was made through the energy transfer from porphyrin excited states to graphene oxide excited states resulting in reduction of singlet state lifetimes of graphene oxide composites. We have done a comprehensive study of graphene oxide with different metal porphyrins and metal free porphyrins for NLA measurements and shown that graphene oxide with metal free porphyrin shows significant nonlinear absorption properties due to the strong electron acceptor capability of the graphene oxide molecule. In comparison with the metal porphyrins with graphene oxide composites, graphene oxide with metal free porphyrin shows high β, and ESA. We also observed that fluorescence quenching is higher for graphene oxide–metal free porphyrin. In ns time scales, composites show good NLA coefficients compared to other regimes. These high NLA coefficients are attributed to the strong TPA, ESA and nonlinear scattering. The composite molecules of graphene oxide and porphyrin have higher FOM values leading to better optical limiting applications. FS results show SA behaviour in all graphene oxide composites indicating that these materials can be used as good saturable absorbers in the fs regime.

Acknowledgements

DNR thanks the Department of Science & Technology sponsored India Trento Program on Advanced Research (ITPAR) for the financial support. One of the authors, MBMK, thanks UGC, Centre for Advanced Studies (CAS) for financial assistance.

References

1 K. S. Novoselov, A. K. Geim, S. V. Morozov, D. Jiang, Y. Zhang, S. V. Dubonos, I. V. Grigorieva and A. A. Firsov, *Science*, 2004, **306**, 666.
2 F. Bonaccorso, Z. Sun, T. Hasan and A. C. Ferrari, *Nat. Photonics*, 2010, **4**, 611.
3 T. Mueller, F. Xia and P. Avouris, *Nat. Photonics*, 2010, **4**, 297.
4 F. Schwierz, *Nat. Nanotechnol.*, 2010, **5**, 487.
5 A. K. Geim and K. S. Novoselov, *Nat. Mater.*, 2007, **6**, 183.
6 C. N. R. Rao, A. K. Sood, K. S. subrahmanyam and A. Govindraj, *Angew. Chem., Int. Ed.*, 2009, **48**, 7752.
7 J. Yang, C. Tian, L. Wang and H. Fu, *J. Mater. Chem.*, 2011, **21**, 3384.
8 W. Xu, L. Zhang, J. Li, Y. Lu, H. Li, Y. Ma, W. Wang and S. Yu, *J. Mater. Chem.*, 2011, **21**, 4593.
9 Y. Liu, J. Zhou, X. Zhang, Z. Liu, X. Wan, J. Tian, T. Wang and Y. Chen, *Carbon*, 2009, **47**, 3113.
10 M. Bala Murali Krishna, V. Praveen Kumar, N. Venkatramaiah, R. Venkatesan and D. Narayana Rao, *Appl. Phys. Lett.*, 2011, **98**, 081106.
11 X. Zhang, X. Zhao, Z. Liu, S. Shi, W. Zhou, J. Tian, Y. Xu and Y. Chen, *J. Opt.*, 2011, **13**, 075202.
12 N. Venkatram, P. Lakshminarayana, M. K. Kumar, B. M. Goh, K. P. Loh, Q. Xu and Wei Ji, *Nanotechnology*, 2010, **21**, 415203.
13 X. Zhang, X. Zhao, Z. Liu, Y. Liu, Y. Chen and J. Tian, *Opt. Express*, 2009, **17**, 23959.
14 Z. Liu, Y. Xu, X. Zhang, Y. Chen and J. Tian, *J. Phys. Chem. B*, 2009, **113**, 9681.
15 Y. Xu, Z. Liu, X. Zhang, Y. Wang, J. Tian, Y. Huang, Y. Ma and Y. Chen, *Adv. Mater.*, 2009, **21**, 1275.
16 M. O. Senge, M. Fazekas, E. G. A. Notaras, W. J. Blau, M. Zawadzka, O. B. Locos and E. M. N. Mhuircheartaigh, *Adv. Mater.*, 2007, **19**, 2737.
17 P. Prem Kiran, D. R. Reddy, A. K. Dharmadhikari, B. G. Maiya, G. R. Kumar and D. N. Rao, *Chem. Phys. Lett.*, 2006, **418**, 442.
18 D. Narayana Rao, *Opt. Mater.*, 2002, **21**, 45.
19 M. Calvete, G. Y. Yang and M. Hanack, *Synth. Met.*, 2004, **141**, 231.
20 S. Keinan, M. J. Therien, D. N. Beratan and W. Yang, *J. Phys. Chem. A*, 2008, **112**, 12203.
21 P. C. Ray and J. Leszczynski, *Chem. Phys. Lett.*, 2006, **419**, 578.
22 E. G. A. Notaras, M. Fazekas, J. J. Doyle, W. J. Blau and M. O. Senge, *Chem. Commun.*, 2007, 2166.
23 T. E. O. Screen, K. B. Lawton, G. S. Wilson, N. Dolney, R. Ispasoiu, T. Goodson III, S. J. Martin, D. C. Bradley and H. L. Anderson, *J. Mater. Chem.*, 2001, **11**, 312.
24 A. D. Adler, F. R. Longo, J. D. Finarelli, J. Goldmacher, J. Assour and L. Korsakoff, *J. Org. Chem.*, 1967, **32**, 476.
25 N. Venkatramaiah and R. Venkatesan, *Solid State Sci.*, 2011, **13**, 616.
26 H. A. Becerril, J. Mao, Z. F. Liu, R. M. Stoltenberg, Z. N. Bao and Y. S. Chen, *ACS Nano*, 2008, **2**, 463.
27 Z. F. Liu, Q. Liu, X. Y. Zhang, Y. Huang, Y. F. Ma, S. G. Yin and Y. S. Chen, *Adv. Mater.*, 2008, **20**, 3924.
28 W. S. Hummers and R. E. Offeman, *J. Am. Chem. Soc.*, 1958, **80**, 1339.
29 A. Das, B. Chakraborty and A. K. Sood, *Bull. Mater. Sci.*, 2008, **31**, 579.
30 Y. Liu, J. Zhou, X. Zhang, Z. Liu, X. Wan, J. Tian, T. Wang and Y. Chen, *Carbon*, 2009, **47**, 3113.
31 Z. Liu, Y. Wang, X. Zhang, Y. xu, Y. chen and J. Tian, *Appl. Phys. Lett.*, 2009, **94**, 021902.
32 Sunil Kumar, M. Anija, N. Kamaraju, K. S. Vasu, K. S. Subrahmanyam, A. K. Sood and C. N. R. Rao, *Appl. Phys. Lett.*, 2009, **95**, 191911.
33 Jingzhi Shang, Zhiqiang Luo, Chunxiao Cong, Jianyi Lin, Ting Yu and Gagik G. Gurzadyan, *Appl. Phys. Lett.*, 2010, **97**, 163103.
34 P. Prem Kiran, D. R. Reddy, B. G. Maiya, A. K. Dharmadhikari, G. R. Kumar and D. N. Rao, *Opt. Commun.*, 2005, **252**, 150.
35 P. Prem Kiran, *Optical limiting and nonlinear optical properties of photo responsive materials: tetratolyporphyrins, pure and iron doped $Bi_{12}SiO_{20}$ crystals and codoped Ag-Cu metal nanoclusters*, PhD Thesis, University of Hyderabad, 2004.

